Nonreciprocal Coupling Induced Self-Assembled Localized Structures

D. Pinto-Ramos,[1] K. Alfaro-Bittner,[2,3] M. G. Clerc,[1] and R. G. Rojas[4]
[1]Departamento de Física and Millennium Institute for Research in Optics, FCFM, Universidad de Chile, Casilla 487-3, Santiago, Chile
[2]Departamento de Física, Universidad Técnica Federico Santa María, Av. España 1680, Casilla 110V, Valparaíso, Chile
[3]Unmanned Systems Research Institute, Northwestern Polytechnical University, Xi'an 710072, China
[4]Instituto de Física, Pontificia Universidad Católica de Valparaíso, Casilla 4059, Valparaíso, Chile

(Received 23 October 2020; accepted 22 March 2021; published 12 May 2021)

Chains of coupled oscillators exhibit energy propagation by means of waves, pulses, and fronts. Nonreciprocal coupling radically modifies the wave dynamics of chains. Based on a prototype model of nonlinear chains with nonreciprocal coupling to nearest neighbors, we study nonlinear wave dynamics. Nonreciprocal coupling induces a convective instability between unstable and stable equilibrium. Increasing the coupling level, the chain presents a propagative pattern, a traveling wave. This emergent phenomenon corresponds to the self-assembly of localized structures. The pattern wavelength is characterized as a function of the coupling. Analytically, the phase diagram is determined and agrees with numerical simulations.

DOI: 10.1103/PhysRevLett.126.194102

The dynamics of coupled oscillators have attracted the attention of physics since its dawn. Phenomena like synchronization [1], energy transfers from one oscillator to another [2], or wave propagation [3] are paradigmatic dynamical behaviors of coupled oscillators. In all the above examples, the oscillators are usually coupled with reciprocal elastic media. Namely, the elastic media are characterized by applying a force of equal magnitude and opposite direction to each of the coupled oscillators. Such dynamical behavior is known as Maxwell-Betti reciprocity [4–6]. Nonreciprocal behavior has been studied in diverse physical fields considering asymmetric, nonlinear, and/or nonreversible features in time. In optics, nonreciprocal responses have been observed in birefringent prisms [7], optomechanical resonators [8], and asymmetric cavities [9]. In acoustics, an emitter and a receiver can exhibit nonreciprocal behaviors in a resonant ring cavity biased by a circulating fluid [10]. A similar phenomenon is achieved for electrically driven nonreciprocity on a silicon chip [11]. Nonreciprocal behaviors for the propagation of electromagnetic waves have been accomplished through the application of magnetic fields [12,13], angular momentum [14], nonlinear coupling [15], and moving photonic crystals [16]. In active matter, nonreciprocal couplings are a rule rather than an exception [17,18]. Recently, through the use of mechanical metamaterials [19,20], nonreciprocal coupling elements have been built up. Namely, couplers that induce a force of different magnitude to the coupled elements. Chains with nonreciprocal couplings exhibit spatially asymmetric standing [21] and nonlinear waves [20]; likewise, localized disturbances tend to propagate more in one direction than another [6–19,21].

In this Letter, we investigate the nonreciprocal coupling effect on nonlinear waves. Based on a prototype model of a nonlinear chain, the dissipative Frenkel-Kontorova model with nonreciprocal coupling to nearest neighbors, a convective instability between unstable and stable steady state is observed. By increasing the level of nonreciprocity, the fronts between these states change from monotonous to nonmonotonous ones. Unexpectedly, beyond a certain nonreciprocity level, fronts become unstable and give rise to propagative patterns (traveling waves), which corresponds to the self-assembly of localized structures. The pattern wavelength is characterized as a function of the couplings. A similar phenomenon is observed in continuous models that include higher spatial derivatives (order four) [22], which accounts for the larger-range coupling and includes a characteristic length. This intrinsic length is the main ingredient of the Turing mechanism of patterns [23,24]. The extension of this phenomenon to discrete systems corresponds to a system coupled to first and second neighbors. It is expected to observe patterns as a result of the intrinsic length provided by more distant neighbors [23,24]. However, the presented pattern mechanism here with nonreciprocal coupling only includes interaction to nearest neighbors. Analytically, the phase diagram of the system is revealed, which shows an excellent agreement with numerical simulations.

Let us consider a dimensionless chain of $N+1$ dissipative coupled pendulums (the dissipative Frenkel-Kontorova model with nonreciprocal coupling [25]):

$$\ddot{\theta}_i = \omega^2 \sin\theta_i - \mu\dot{\theta}_i + (D-\alpha)(\theta_{i+1}-\theta_i) - (D+\alpha)(\theta_i-\theta_{i-1}), \quad (1)$$

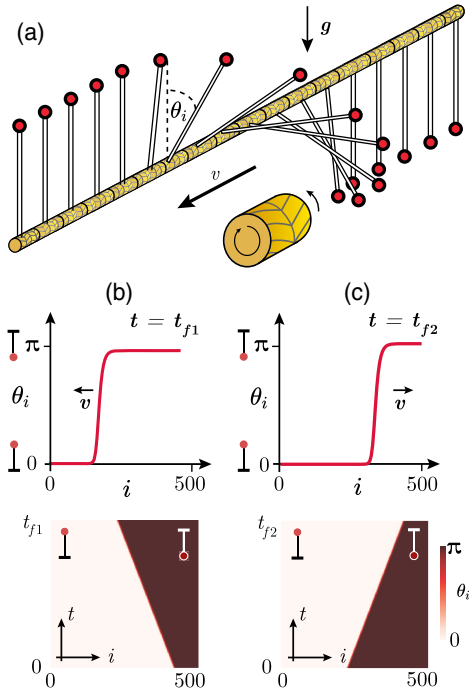

FIG. 1. Nonreciprocal coupled chain of pendulums and front propagation. (a) Schematic representation of a chain of pendulums coupled with a nonreciprocal material. $\theta_i(t)$ is the angle formed by the pendulum and the vertical axis in the i position at time t. Yellow cylinder accounts for a nonreciprocal metamaterial. Instantaneous profile and spatiotemporal evolution of π kink obtained for Eq. (2) with $\omega = 1$, $D = 4$, $\alpha = 1$ (b), and $\alpha = 2.5$ (c).

where $\theta_i(t)$ is the angle formed by the pendulum and the vertical axis in the i position at time t [cf. Fig. 1(a)]. ω and μ are the natural frequency and the damping coefficient of pendulums. D and α account for coupling elements that have different left-to-right and right-to-left linear responses. α accounts for the nonreciprocal coupling; when $\alpha = 0$, the chain has a reciprocal coupling. D stands for the linear deformation of an elastic material. α could account for the linear deformations of a rubber nonreciprocal torsion metamaterial [19] or a nonreciprocal robotic coupling [21]. Figure 1 shows a schematic representation of a chain of dissipative coupled pendulums. Note that $\theta_i = 0$ and $\theta_i = \pi$ describe the upside-down and upright pendulum, respectively. Equation (1) is of Lagrangian nature, which has the form

$$\mathcal{L} = \sum_i \left[\frac{\dot{\theta}_i^2}{2} - \omega^2 \cos\theta_i - \frac{D-\alpha}{2}(\theta_{i+1} - \theta_i)^2\right] e^{\mu t}\Lambda^i,$$

where $\Lambda \equiv (D-\alpha)/(D+\alpha)$. Thereby, the dynamics of Eq. (1) is steered by a principle of least action. To figure out the nonreciprocal chain dynamics, we consider the overdamped limit of the dissipative Frenkel-Kontorova model (see the Supplemental Material [26]). Then Eq. (1) can be approximated by

$$\dot{\theta}_i = \omega^2 \sin\theta_i + (D-\alpha)(\theta_{i+1} - \theta_i) - (D+\alpha)(\theta_i - \theta_{i-1}). \tag{2}$$

A similar model was proposed to study coupled Josephson junctions [29]. Two evident extended steady states correspond to the uniform upside-down and upright pendulums. To study the dynamics of nonlinear waves between these two states, we consider the boundary conditions being Dirichlet $[\theta_0(t) = 0]$ and Neumann $[\theta_N(t) = \theta_{N-1}(t)]$ on the left and right flank of the chain, respectively.

In the reciprocal limit $\alpha = 0$, considering all upside-down pendulums as an initial condition, slightly tilting a pendulum generates a nonlinear wave that propagates from the upright to the upside-down pendulums with a well-defined speed. This nonlinear wave is known as π kink [30]. The front speed is characterized by exhibiting a weakly oscillatory behavior [30,31]. π kinks are persistent in the presence of nonreciprocal coupling. Figure 1 shows the profile of a π kink wave and its respective spatiotemporal diagram. These diagrams were obtained by means of numerical simulations. All the numerical simulations presented were conducted by a fourth-order Runge-Kutta integration method. As a result of nonreciprocal coupling, the speed of the π kink decreases when α is increased. π kinks that invade the upside-down pendulums are observed in zone I of Fig. 2. The previous dynamical behaviors change when considering large enough α through an absolute convective instability [32]; the upside-down pendulums invade upright ones [see Fig. 1(c)]. These fronts are observed in zone II on the bifurcation diagram in Fig. 2.

To characterize the absolute convective instability, we use the same strategy presented in [30]. Let us introduce the ansatz $\theta_i(t) = Ae^{k(i+\langle v\rangle t)}$ for the tail of the front to determine the average front speed $\langle v\rangle$, where k accounts for the front steepness. The average front speed $\langle v\rangle$ satisfies (see the Supplemental Material [26] for details)

$$\langle v(k)\rangle = \frac{\omega^2 - 2D}{k} + 2\left[\frac{D\cosh(k) - \alpha\sinh(k)}{k}\right]. \tag{3}$$

Bounded disturbances induce fronts propagation into the unstable state with the minimum front speed $v_{\min}$ as a function of the steepness, i.e., $v_{\min} = \langle v(k = k_c)\rangle$, $\partial_k\langle v(k = k_c)\rangle = 0$, and $\partial_{kk}\langle v(k = k_c)\rangle > 0$ [22]. The absolute convective instability corresponds when the minimum speed is zero [32]. Using this condition, we get

$$D = \frac{\alpha^2}{\omega^2} + \frac{\omega^2}{4}. \tag{4}$$

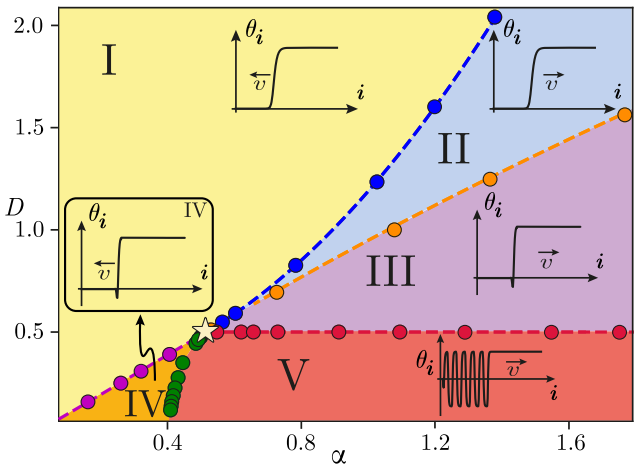

FIG. 2. Phase diagram of the overdamped Frenkel-Kontorova Eq. (2) with $\omega = 1$. In zone I, the upright pendulums invade the upside-down ones. This process is reversed in zone II. The blue curve, Eq. (4), is the analytical absolute convective instability between the upright and upside-down pendulums. The purple ($D = \alpha$) and orange curves account for the monotonous to nonmonotonous front transition, using Eq. (3). The star symbol (☆) accounts for the critical point ($\alpha = 1/2, D = 1/2$) where the critical curves converge. Red and green curves separate the localized structures' self-assembly region. The red curve was obtained using formula $D = 1/2$. The green curve is achieved through divergence of the self-assembly wavelength. All circles are obtained by means of numerical simulations.

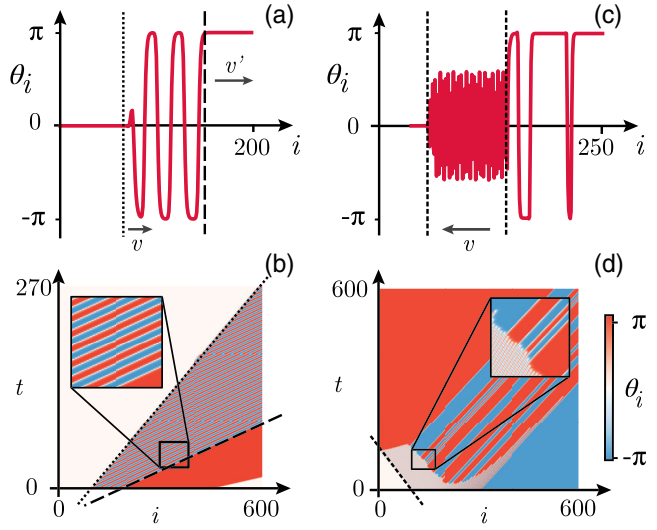

FIG. 3. Nonmonotonous fronts of the overdamped Frenkel-Kontorova Eq. (2) with $\omega = 1$. Profile (a) and spatiotemporal evolution (b) of a nonmonotonous front propagates from upside-down pendulums into upright ones for $D = 1$ and $\alpha = 1.25$. v and v' account for the speeds of different fronts. Profile (c) and spatiotemporal evolution (d) of a nonmonotonous front propagate from upright pendulums into upside-down pendulums for $D = 0.25$ and $\alpha = 0.325$.

Figure 2 shows the bifurcation diagram of the overdamped Frenkel-Kontorova model, Eq. (2). The dashed blue curve accounts for the previous expression. Notice that for large D coupling, the system is adequately described by the continuous limit, the dissipative sine-Gordon equation with advection, where the dynamic behaviors described above are expected. Surprisingly, as α increases further, the fronts exhibit a transition from monotonous to nonmonotonous fronts. Figure 3 shows the typical nonmonotonous front observed and its propagation. These fronts are observed in zones III and IV of the phase diagram shown in Fig. 2. In zone III (IV), the upside-down (upright) state propagates into the upright (upside-down) one. The transition of monotonous to nonmonotonous front is characterized by the fact that the speed curve $\langle v(k)\rangle$, Eq. (3), ceases to have a minimum, which becomes an inflection point. Indeed, the minimum is now in the complex plane of k, where the imaginary part corresponds to the spatial oscillations observed in the front profile (cf. Fig. 3). By imposing that $\langle v(k = k_c)\rangle$ stops having a minimum, we obtain

$$\frac{2D - \omega^2}{\operatorname{arctanh}(\frac{D}{\alpha})} = 2\alpha\sqrt{1 - \left(\frac{D}{\alpha}\right)^2}. \tag{5}$$

For $D < \omega^2/2$, an explicit solution of the above transcendent equation is $D = \alpha$. Notice that this relationship corresponds to each oscillator being only coupled to its left neighbor. Furthermore, when $D < \alpha$, springs toward the right side are not of restoring nature, that is, their elastic constant is negative. The above is unacceptable for mechanical springs. However, this type of coupling can be achieved through the use of nonreciprocal robotic metamaterials [21]. For $D > \omega^2/2$, an explicit analytic expression is not accessible. Note that the curve obtained parametrically, Eq. (5), is slightly below the straight line $D = \alpha$. Figure 2 illustrates these curves by means of the purple and orange dashed lines, respectively. $D = \alpha = \omega^2/2$ is a critical point where the different transition curves converge, which is represented by a star in the phase diagram of Fig. 2. From nonmonotonous fronts where the upside-down pendulum state invades upright ones, unexpectedly, as D decreases, the emergence of a traveling wave is observed (see Fig. 4). Note that these patterns are characterized by connecting the vertical pendulum to itself. These propagative waves are observed in zone V on the phase diagram of Fig. 2. As α is increased or D is decreased, the wavelength of the propagative pattern λ decreases as illustrated in Fig. 4(c). To characterize the pattern emergence instability curve, we consider nonmonotonous fronts where upside-down pendulums invade upright ones. The average front speed $\langle v(k_c)\rangle$ is the global minimum as a function of steepness. Using the previous conditions in Eq. (3) after straightforward calculations (for details, see the Supplemental Material [26]), we obtain the relation $D = \omega^2/2$. The red dashed horizontal line in Fig. 2 outlines the wave instability curve. Increasing the number of

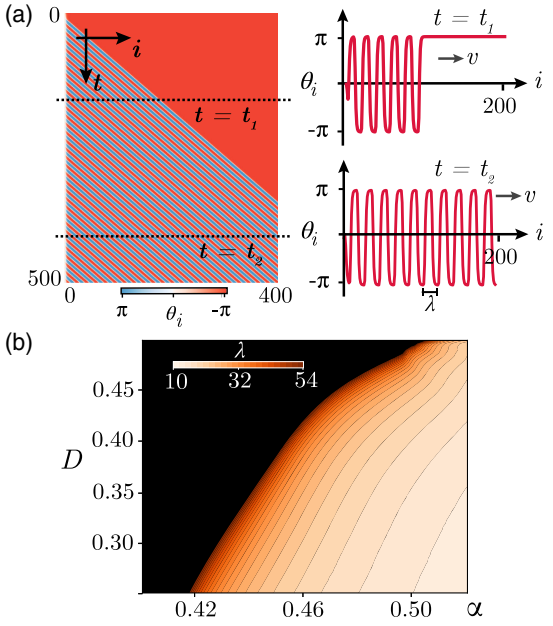

FIG. 4. Self-assembly of localized structures and the wavelength surface map for the overdamped Frenkel-Kontorova Eq. (2) with $D = 0.4$, $\alpha = 0.5$, and $\omega = 1$. (a) Spatiotemporal evolution and respective profiles in two instants of time, $t_1 = 120$ and $t_2 = 395$. v accounts for the traveling wave velocity. (b) Wavelength surface map for the D and α parameter space.

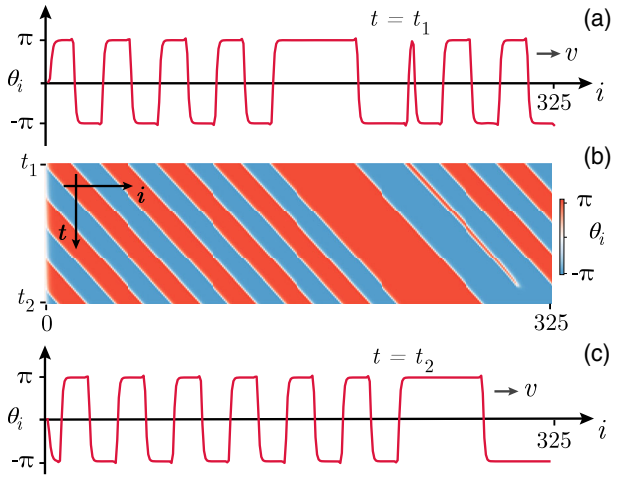

FIG. 5. Self-assembly of localized structures obtained for the overdamped Frenkel-Kontorova Eq. (2) with $D = 0.25$, $\omega = 1$, and $\alpha = 0.425$. (b) Spatiotemporal evolution of Eq. (2) with initial condition top panel (a) and final state bottom panel (c). v stands for the speed of the ensemble of localized structures.

oscillators N close to the horizontal line, numerically, we observe that the wave exhibits a complex spatiotemporal dynamics. The origin and the characterization of the complex spatiotemporal behavior is in progress.

The transition between fronts and large wavelength waves (zones IV and V) cannot be obtained employing asymptotic analytical calculations due to its nonlinear nature. To determine this bifurcation, we numerically compute the curve of divergence of the pattern wavelength. Figure 2 illustrates this curve by means of green dots. Video in the Supplemental Material [26] illustrates the different observed nonlinear waves [33]. To shed light on the nature of the observed patterns, we perturb the periodic solution in a localized manner. The spatial oscillations with a length small enough compared to the pattern shrink and disappear, generating a hole in the pattern that propagates without deformation. In contrast, oscillations with a wavelength longer than the pattern, even several wavelengths, propagate as a localized state, a *pulse*. Figure 5 illustrates the scenario described above. A pattern made up of an extended periodic state is characterized by healing the disturbances and recovers the pattern characteristic wavelength [23,24]. However, patterns composed by the assembly of localized structures are characterized by exhibiting various wavelengths and configurations, depending on the initial condition [33]. When one regards a localized solution as an initial condition, it is propagated and advected. Because of the fixed boundary condition, localized structures of equal size begin to be emitted from the left flank, forming the propagative pattern. Therefore, the observed propagative pattern corresponds to a self-assembly of propagative localized structures (cf. Fig. 5).

The origin of the emergence of the observed pattern is that the front between the upright and upside-down pendulums has a well-defined periodic length when it tends to the fixed edge, left flank. This front profile engenders alternation of domains of the π and $-\pi$ states. Indeed, it locally generates a 2π kink gas. The interaction between these particle-type solutions is responsible for localized states [34]. Moreover, their interaction is characterized by exhibiting a family of localized solutions displaying a complex bifurcation diagram, a *collapsed snaking bifurcation*. Spontaneously from the left edge, there is an emission of localized solutions of one width. However, all localized solutions with greater width are observed (stable) when adequate initial conditions are considered.

When inertia is included, i.e., in the underdamped regime, the phenomena presented above persist. In fact, the phase diagram presented in Fig. 2 is slightly modified (for more details, see the Supplemental Material [26]).

In conclusion, based on a prototype model of a nonlinear oscillator chain with a nonreciprocal coupling to nearest neighbors, a convective instability between unstable and stable equilibrium is studied. By increasing the level of nonreciprocity coupling, fronts between these states exhibit a transition from monotonous to nonmonotonous fronts. Unexpectedly, as the level of nonreciprocity increases, fronts become unstable and give rise to propagative patterns with a wavelength controllable by coupling, which corresponds to self-assembly of localized structures. Analytically, the phase diagram of the system is revealed.

Because of the universal nature of the model under study, we expect that the presented findings are generic. Namely, we expect to observe the self-assembled localized structures in various nonlinear oscillators with nonreciprocal coupling. Josephson junctions, coupled with nonreciprocal robotic elements or computer-assisted coupling, are possible experiments that could display the proposed phenomena. In the case of considering large deformations of rubber nonreciprocal metamaterial, one would expect a nonreciprocal nonlinear coupling. The study of this type of coupling on the dynamics of waves is a work still in progress. In the continuous limit, the nonreciprocal coupling is only responsible for the absolute convective instability between fronts. Instead, the emergence of self-assembly of localized structures is a peculiar phenomenon of nonreciprocally coupled to nearest neighbor systems.

This work was funded by ANID-Millennium Science Initiative Program–ICN17_012. M. G. C. acknowledges financial support from the Fondecyt 1210353 project. D. P. R. acknowledges financial support from the ANID national Ph.D. scholarship 21201484.

[1] A. Pikovsky, J. Kurths, M. Rosenblum, and J. Kurths, *Synchronization: A Universal Concept in Nonlinear Sciences*, Vol. 12 (Cambridge University Press, Cambridge, England, 2003).
[2] J. P. Den Hartog, *Mechanical Vibrations* (Dover Publications, New York, 1985).
[3] A. L. Fetter and J. D. Walecka, *Theoretical Mechanics of Particles and Continua* (Dover Publications, New York, 2003).
[4] J. C. Maxwell, On the calculation of the equilibrium and stiffness of frames, Philos. Mag. Ser. 5 **27**, 294 (1864).
[5] E. Betti, Teoria della elasticita, Il Nuovo Cimento **7–8**, 158 (1872).
[6] H. Nassar, B. Yousefzadeh, R. Fleury, M. Ruzzene, A. Alù, C. Daraio, A. N. Norris, G. Huang, and M. R. Haberman, Nonreciprocity in acoustic and elastic materials, Nat. Rev. Mater. **5**, 667 (2020).
[7] L. Alekseeva, I. Povkh, V. Stroganov, B. Kidyarov, and P. Pasko, A nonreciprocal optical element, J. Opt. Technol. **70**, 525 (2003).
[8] I. M. Mirza, W. Ge, and H. Jing, Optical nonreciprocity and slow light in coupled spinning optomechanical resonators, Opt. Express **27**, 25515 (2019).
[9] P. Yang, X. Xia, H. He, S. Li, X. Han, P. Zhang, G. Li, P. Zhang, J. Xu, Y. Yang *et al.*, Realization of Nonlinear Optical Nonreciprocity on a Few-Photon Level Based on Atoms Strongly Coupled to an Asymmetric Cavity, Phys. Rev. Lett. **123**, 233604 (2019).
[10] R. Fleury, D. L. Sounas, C. F. Sieck, M. R. Haberman, and A. Alù, Sound isolation and giant linear nonreciprocity in a compact acoustic circulator, Science **343**, 516 (2014).
[11] H. Lira, Z. Yu, S. Fan, and M. Lipson, Electrically Driven Nonreciprocity Induced by Interband Photonic Transition on a Silicon Chip, Phys. Rev. Lett. **109**, 033901 (2012).
[12] Z. Wang, Y. Chong, J. D. Joannopoulos, and M. Soljačić, Observation of unidirectional backscattering-immune topological electromagnetic states, Nature (London) **461**, 772 (2009).
[13] F. D. M. Haldane and S. Raghu, Possible Realization of Directional Optical Waveguides in Photonic Crystals with Broken Time-Reversal Symmetry, Phys. Rev. Lett. **100**, 013904 (2008).
[14] D. L. Sounas, C. Caloz, and A. Alù, Giant non-reciprocity at the subwavelength scale using angular momentum-biased metamaterials, Nat. Commun. **4**, 2407 (2013).
[15] S. Lepri and G. Casati, Asymmetric Wave Propagation in Nonlinear Systems, Phys. Rev. Lett. **106**, 164101 (2011).
[16] D.-W. Wang, H.-T. Zhou, M.-J. Guo, J.-X. Zhang, J. Evers, and S.-Y. Zhu, Optical Diode Made from a Moving Photonic Crystal, Phys. Rev. Lett. **110**, 093901 (2013).
[17] M. Nagy, Z. Ákos, D. Biro, and T. Vicsek, Hierarchical group dynamics in pigeon flocks, Nature (London) **464**, 890 (2010).
[18] F. Ginelli, F. Peruani, M.-H. Pillot, H. Chaté, G. Theraulaz, and R. Bon, Intermittent collective dynamics emerge from conflicting imperatives in sheep herds, Proc. Natl. Acad. Sci. U.S.A. **112**, 12729 (2015).
[19] C. Coulais, D. Sounas, and A. Alù, Static non-reciprocity in mechanical metamaterials, Nature (London) **542**, 461 (2017).
[20] L. Jin, R. Khajehtourian, J. Mueller, A. Rafsanjani, V. Tournat, K. Bertoldi, and D. M. Kochmann, Guided transition waves in multistable mechanical metamaterials, Proc. Natl. Acad. Sci. U.S.A. **117**, 2319 (2020).
[21] M. Brandenbourger, X. Locsin, E. Lerner, and C. Coulais, Non-reciprocal robotic metamaterials, Nat. Commun. **10**, 4608 (2019).
[22] W. Van Saarloos, Front propagation into unstable states, Phys. Rep. **386**, 29 (2003).
[23] L. M. Pismen, *Patterns and Interfaces in Dissipative Dynamics* (Springer Science & Business Media, New York, 2006).
[24] M. Cross and H. Greenside, *Pattern Formation and Dynamics in Nonequilibrium Systems* (Cambridge University Press, Cambridge, England, 2009).
[25] O. M. Braun and Y. S. Kivshar, *The Frenkel-Kontorova Model: Concepts, Methods, and Applications* (Springer Science & Business Media, New York, 2013).
[26] See Supplemental Material, which includes Refs. [27,28], at http://link.aps.org/supplemental/10.1103/PhysRevLett.126.194102 for detailed calculations and the inertia term effect. See video in the Supplemental Material [26]. The movie shows the different fronts and traveling waves exhibited by the dissipative Frenkel-Kontorova model with nonreciprocal coupling.
[27] L. Jin, R. Khajehtourian, J. Mueller, A. Rafsanjani, V. Tournat, K. Bertoldi, and D. M. Kochmann, Guided transition waves in multistable mechanical metamaterials, Proc. Natl. Acad. Sci. U.S.A. **117**, 2319 (2020).
[28] S. H. Strogatz, *Nonlinear Dynamics and Chaos: With Applications to Physics, Biology, Chemistry and Engineering* (Addison-Wesley, Reading, MA, 1994).
[29] E. Trias, J. J. Mazo, F. Falo, and T. P. Orlando, Depinning of kinks in a Josephson-junction ratchet array, Phys. Rev. E **61**, 2257 (2000).

[30] K. Alfaro-Bittner, M. G. Clerc, R. G. Rojas, and M. A. García-Ñustes, Traveling wave into an unstable state in dissipative oscillator chains, Nonlinear Dyn. **98**, 1391 (2019).

[31] K. Alfaro-Bittner, M. G. Clerc, M. A. García-Ñustes, and R. G. Rojas, π-kink propagation in the damped Frenkel-Kontorova model, Europhys. Lett. **119**, 40003 (2017).

[32] E. Lifschitz and L. Pitajewski, Physical kinetics, in *Textbook of Theoretical Physics. 10* (Akademie-Verlag, Berlin, 1983), https://inis.iaea.org/search/search.aspx?orig_q=RN:15057084.

[33] E. Berríos-Caro, M. Clerc, D. Escaff, C. Sandivari, and M. Tlidi, On the repulsive interaction between localised vegetation patches in scarce environments, Sci. Rep. **10**, 5740 (2020).

[34] P. Coullet, Localized patterns and fronts in nonequilibrium systems, Int. J. Bifurcation Chaos Appl. Sci. Eng. **12**, 2445 (2002).